Protonation, Photobleaching, and Photoactivation of Yellow Fluorescent Protein (YFP 10C): A Unifying Mechanism†

Tim B. McAnaney,‡ Wei Zeng,# Camille F. E. Doe,# Nina Bhanji,# Stuart Wakelin,# David S. Pearson,§ Paul Abbyad,‡ Xinghua Shi,‡ Steven G. Boxer,‡ and Clive R. Bagshaw*,#

Department of Chemistry, Stanford University, Stanford CA94305, Department of Biochemistry, University of Leicester, Leicester LE1 7RK, U.K., and Department of Biosciences, University of Kent, Canterbury, Kent CT2 7NJ, U.K.

Received November 17, 2004; Revised Manuscript Received February 7, 2005

ABSTRACT: Yellow fluorescent protein (YFP 10C) is widely used as a probe in biology, but its complex photochemistry gives rise to unusual behavior that requires fuller definition. Here we characterize the kinetics of protonation and reversible bleaching over time scales of picoseconds to hours. Stopped-flow and pressure-jump techniques showed that protonation of the fluorescent YFP^- anion state is two-step with a slow transition that accounts for blinking of 527 nm emission at the single molecule level on the seconds time scale. Femtosecond spectroscopy revealed that the protonated excited-state (YFPH*) decayed predominantly by a radiationless mechanism, but emission at 460 nm was detected within the first picosecond. Limited excited-state proton transfer leads to 527 nm emission characteristic of the YFP^{-}* anion. Prolonged continuous wave illumination at the peak of YFP^- absorbance (514 nm) yields, irreversibly, a weakly fluorescent product that absorbs at 390 nm. This "photobleaching" process also gives a different species (YFPHrb) that absorbs at 350/430 nm and spontaneously regenerates YFP^- in the dark on the time scale of hours but can be photoactivated by UV light to regenerate YFP^- within seconds, via a ground-state protonated intermediate. Using a pulsed laser for photobleaching resulted in decarboxylation of YFP as indicated by the mass spectrum. These observations are accounted for in a unifying kinetic scheme.

Green fluorescent protein (GFP)[1] and its color variants have found wide use in biology to probe protein dynamics in vitro and within cells (*1*). They have also attracted the attention of spectroscopists owing to their complex photochemistry (*2*−*5*). In particular, those in the YFP class (i.e. containing a T203Y or T203F mutation to shift the emission to 527 nm) have been shown to undergo fluctuations of emission intensity over a wide range of times scales and reversible photobleaching (*6*−*8*). Fluctuations in emission were observed by wide field microscopy at the single molecule level by immobilizing individual YFP molecules in acrylamide or agarose gels and using TIRF excitation (*6*, *9*). Molecules were found to blink on the seconds time scale at low laser powers (<500 W cm^{-2}). Increasing laser power reduced the lifetime of the emitting state, but not in direct proportion to the laser power. Initial studies discussed the possibility that the fluctuations were related to the protonation of the phenolate moiety of the fluorophore derived from Y66 (*6*), but later studies found little pH dependence of the on- and off-times when monitored at a laser power of 5000 W cm^{-2} (*9*).

Members of the YFP class also showed a photochromic switching behavior. Molecules that were bleached by 488 nm irradiation, could be induced to fluoresce by illumination with near UV or blue light (*6*−*8*). This reversible photobleaching reaction of YFP was observed in FRET measurements (*10*). Illumination of YFP at 514 nm resulted in bleaching of the YFP acceptor and dequenching of a donor CFP molecule. Once the YFP was bleached, illumination in the 330−390 nm region resulted in partial recovery of the initial YFP fluorescence and resumed FRET with the CFP moiety.

Despite these and other spectroscopic studies of YFP, the photochemical events involved have not been completely rationalized into a unifying scheme with respect to the ground-state species. Here we report on the properties of the YFP 10C variant containing the substitutions S65G, V68L, S72A and T203Y. This construct has been widely used as a result of its commercial availability. Our interest in this protein arose from its use as a probe for actomyosin kinetics. We attempted to follow the ATP-induced dissociation of a YFP-myosin motor fusion protein from a single

† This work was supported by the Biotechnology and Biological Sciences Research Council and the Wellcome Trust in the U.K. The work at Stanford was supported, in part, by a grant from the NIH (Grant GM27738). The fluorescence upconversion facilities are supported by the Medical Free Electron Laser Program of the Air Force Office of Scientific Research (Grant No. F49620-00-1-0349).

* To whom correspondence should be addressed. Tel: +44 (0)116 252 3454. Fax: +44 (0)116 252 3369. E-mail: crb5@le.ac.uk.

‡ Stanford University.

University of Leicester.

§ University of Kent.

[1] Abbreviations: CFP, cyan fluorescent protein; CW, continuous wave; FRET, fluorescence resonance energy transfer; GFP, green fluorescent protein; HEPES, *N*-(2-hydroxyethyl)piperazine-*N*′-(2-ethanesulfonic acid); IRF, instrument response function; MES, 2-(*N*-morpholino)ethanesulfonic acid; MOPS, (3-(*N*-morpholino)propanesulfonic acid; TCSPC, time-correlated single photon counting; TIRF, total internal fluorescence reflection fluorescence; XFP, irreversibly bleached YFP; YFP, yellow fluorescent protein.

10.1021/bi047581f CCC: $30.25
Published on Web 03/12/2005

actin filament by TIRF microscopy using flash photolysis of caged ATP (*11*). In control experiments we noted that the UV flash from the Xe lamp caused photoactivation of the partially bleached YFP-myosin fusion protein. Interestingly, the fluorescence recovered on the time scale of around 1 s, significantly longer than the flash itself. Thus the photoactivation pathway must involve an additional dark state before producing the fluorescent YFP species. Here we report on the time scale and pH dependence of the ground-state reactions and relate them to the previous studies to arrive at an overall photochemical scheme that links the protonation of YFP, the blinking reaction and the photoactivation process. We also carried out ultrafast spectroscopic measurements to follow the proton-transfer reactions of the excited state and found similarities and differences with previous studies on GFP (*2*).

MATERIALS AND METHODS

YFP Cloning and Preparation. YFP (Clontech EYFP; BD Biosciences, Oxford, UK) was expressed with a His tag at its N terminal in *E. coli*, strain BL21, using a pET28a+ expression vector (Novagen: Merck Biosciences, Beeston, U.K.). This protein corresponds to the 10C mutant (*1*) and has substitutions at S65G, V68L, S72A and T203Y. The protein was purified under native conditions on a Ni −NTA affinity agarose column (Qiagen, Crawley, U.K.). Mass spectrometry revealed a molecular weight of 29,004 which indicated that the initial methionine residue was absent, and confirmed that the N-terminal sequence was (M)GSSHHHHHHSSGLVPRGSH**MVSKG ...**, where residues in bold represent those of YFP itself.

The YFP-myosin motor construct was made by fusing YFP (Clontech) with the N terminus of the *Dictyostelium discoideum* W501+ myosin II construct (*12*). No linker region was included so that the YFP sequence (in bold) and myosin sequence were contiguous (i.e. ....**MDELYK**DPIHDR....). The protein was expressed in the pDXA-3H vector that incorporated a His_8 tag at the C-terminus of the myosin motor domain to aid purification. *Dictyostelium* culture and protein purification was carried out as previously described (*12*).

Proteins were dissolved in a buffer of 40 mM NaCl, 2 mM $MgCl_2$, and 20 mM buffer (MOPS, HEPES or MES depending on pH required). For deuterated buffer solutions, the buffer was made up in D_2O and adjusted to the final pD using DCl or NaOD. Buffers were corrected for the isotope effect on the pH meter (*13*).

Steady-State Spectroscopy and Photobleaching. Absorption and fluorescence spectra were recorded using a Cary 50 spectrophotometer and Eclipse spectrofluorometer respectively (Varian Ltd, Walton-on-Thames, U.K.). A 150 μL sample was placed into a Hellma 105.250-QS Suprasil cuvette with a path length of 10 mm and 2 × 5 mm windows for absorption measurement, laser and Xe flash lamp irradiation. For fluorescence measurements the sample was excited in the same cell but through the side window (i.e. 2 mm path length) to reduce inner filter effects. Stopped-flow measurements were made using a SX18MV instruments (Applied Photophysics Ltd, Leatherhead, U.K) equipped with photomultiplier or diode array detectors. Pressure-jump experiments were performed on a custom-built apparatus using a piezoelectric crystal stack (P-245.70, Physik Instrumente GmbH, Waldbronn, Germany) to apply rapid pressure (5 to 8 MPa) increases and releases to a 50 μL sample, as described previously (*14*). YFP emission was measured using 514 nm excitation and a 530 nm cutoff filter, in both stopped-flow and pressure-jump experiments. Transient kinetic records were analyzed using Kaleidagraph (Synergy Software, Pennsylvania). Concentrations refer to the reaction chamber, unless otherwise stated. In general, forward rate constants are denoted k_i and reverse rate constants k_{-i} with an equilibrium constant K_i. Protonation reactions are described using association equilibrium constants, and thus the reciprocal K is used to define pK values. In kinetic schemes in which excited-state processes contribute to the flux, the absorption process is described by an operational rate constant $k_i \epsilon I$, where ϵ is the absorption coefficient and I is the light intensity.

Photobleaching in the Leicester laboratory was achieved using 250 mW of 514 nm CW light from a Lexel 85−1 argon ion laser (Lambda Photometrics, Harpenden, U.K.). Photoactivation was induced with a Xe XF-10 flash lamp (Hi-Tech, Salisbury, U.K.) using a range of UV band-pass interference filters. Additionally, a comparison of photobleaching by different excitation sources was undertaken in the Stanford laboratory by exciting the YFP samples at pH 8 for ∼ 30 min. with 30 mW of 532 nm light at 10 Hz (3 mJ/pulse, 6−7ns pulse width) by a Quanta Ray INDI-30 Nd:YAG laser (Spectra Physics, Mountain View, CA), with 750 mW of 532 nm CW light by an Millenium V Nd:YVO_4 laser (Spectra Physics) and with 250 mW of 514 nm CW light by a Model 95 argon-ion laser (Lexel, Freemont, CA). Absorption spectra of these samples were recorded on a Lambda 12 UV/vis spectrophotometer (Perkin-Elmer). Electrospray mass spectra (Waters Micromass ZQ) were taken of the YFP samples before and after photobleaching.

Ultrafast, Time-Resolved Spectroscopy. The time-resolved fluorescence emission of YFP was measured at 460 and 525 nm by an integrated fluorescence upconversion (*2*, *15*) and TCSPC setup which will be described in detail elsewhere. Briefly, the YFP samples were excited by a 400 nm excitation pulse generated from the second harmonic of an argon-ion pumped titanium:sapphire laser. The IRF measured with scattered excitation light was typically ∼160 fs by fluorescence upconversion and 30 ps by TCSPC and the respective time windows of data acquisition were 1.3 and 10 ns. The sample, stirred continuously in a 1-mm path length quartz cuvette, was excited at 82 MHz with 10 mW (12 pJ/pulse) of light polarized at the magic angle with respect to either the gate beam and BBO crystal (for upconversion) or a Glan-Thomson polarizer in the emission path (for TCSPC). In upconversion, a UG11 (Schott Glass Technologies, PA) filter provided good transmission of the upconverted light over the desired wavelength range (290−320 nm) while sufficiently blocking the nonupconverted fluorescence and residual, scattered 400 nm excitation light. In TCSPC, a 420 nm long-pass filter provided efficient transmission of the fluorescence emission and sufficiently blocked scattered excitation light at 400 nm. Time-resolved fluorescence was detected by an R3809U-50 MCP (Hamamatsu) and an SPC-630 TCSPC module (Becker & Hickl, Germany) through the second port of the 270M dual-port monochromator (Spex Industries, NJ). For anisotropy scans, the excitation beam was rotated with a 1/2 λ-plate to parallel and perpendicular

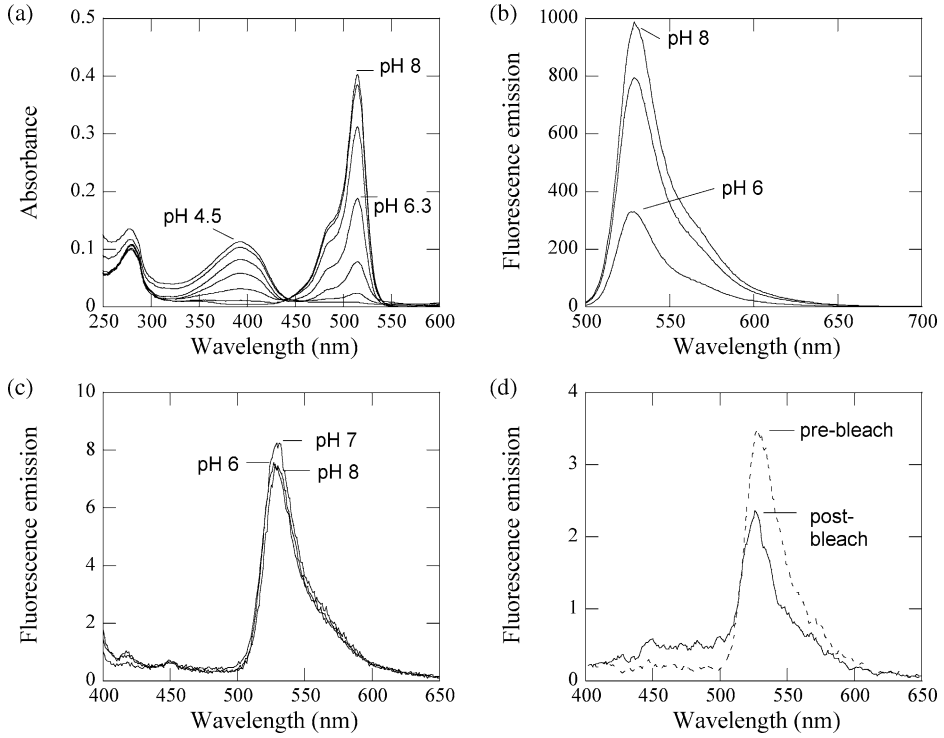

FIGURE 1: Absorption and fluorescence emission spectra of YFP. (a) Absorption spectra of 4.8 μM YFP as a function of pH. The spectra were obtained at pH 8, 7.3, 6.7, 6.3, 5.7, 5.2 and 4.5 and show a decreasing absorbance at 514 nm to yield a p*K* of 6.3 (see Figure 2c) in 40 mM NaCl, 2 mM $MgCl_2$ and 5 mM TES 15 mM MES buffer at 20 °C (pH adjusted with acetic acid). (b) Fluorescence emission spectra (excitation at 480 nm) for similar YFP sample at pH 8, 7 and 6. (c) same samples as in (b) but with 390 nm excitation − note the reduction in intensity by 2 orders of magnitude and the lack of emission in the region 450−500 nm. (d) Fluorescence emission spectra (390 nm excitation) of a sample of YFP at pH 7.2 before (dashed line) and after (solid line) 10 min exposure to 514 nm laser light to effect 80% photobleaching. Note the appearance of a weak broad peak in the region 450−500 nm.

polarizations and the time-resolved anisotropy was calculated as $r(t) = [(I_{||}(t) - I_{\perp}(t))/(I_{||}(t) + 2I_{\perp}(t))]$.

At pH 6, the excited-state dynamics were monitored in both protonated and deuterated buffer solutions and at pH 8, the excited-state dynamics were examined before and after photobleaching. Photobleaching was achieved by exposing the sample to 532 nm pulses from the Nd:YAG laser (described above) for approximately 1 h. In addition, the time-resolved fluorescence spectrum of YFP at pH 6 in protonated buffer was recorded by fluorescence upconversion spectroscopy at $t = 0.3$ and 10 ps using a method adopted from Gustavsson et al. (*16*). The phase matching angle for sum frequency generation was tuned with the monochromator detection wavelength while fine adjustments of the delay line compensated for the group velocity mismatch of the different spectral components traveling through the sample cuvette and the BBO crystal. The spectrum recorded at $t = -1$ ps was subtracted from the spectra collected at positive time delays.

Microscopy. The TIRF microscope has been described in detail previously (*17*, *18*) and is based on a Zeiss 135TV axiovert microscope with a 63 × 1.2 N.A. C-apochromat water immersion objective lens. A Lexel 85−1 argon ion laser was used to excite YFP at 514 nm using the prism TIRF method. The polarization of the laser beam was rotated through 90° by a Fresnel rhomb prism to become perpendicular to the plane of incidence (s-polarization). Laser powers were measured at the entrance to the prism using a LaserCheck meter (Coherent, Watford, U.K.) and the power of the evanescent field at the silica-water interface was calculated from the area of illumination (approximately 60 × 160 μm ellipse) and the appropriate equation (*19*, *20*). YFP emission was detected through an Omega545AF35 filter (Glen Spectra Ltd, Stanmore, U.K.). Single molecules of YFP were imaged at video rate (25 Hz) using an IC-300 ICCD camera (PTI, Surbiton, U.K.) and captured using an LG3 frame grabber (Scion Corporation, Frederick, MD). The intensity of individual spots with time was analyzed using Scion NIH image software. Autocorrelation analysis of the fluctuations was performed in an Excel spreadsheet using the Fast Fourier Transform routine (*21*). Photoactivation was induced with a Xe XF-10 flash lamp, with a 280 to 380 nm band-pass interference filter as described previously (*18*).

RESULTS

Absorption and Fluorescence Spectra. Figure 1a shows the pH dependence of the YFP absorption spectra in a buffer comprising 40 mM NaCl, 2 mM $MgCl_2$ and 20 mM MES/TES buffer at 20 °C. As shown previously (*22*, *23*), the anionic YFP^- species has a peak in absorption at 514 nm, while the protonated form has a peak at 390 nm with an isobestic point at 438 nm. Below pH 5.5 there was a slight rise in turbidity due to limited denaturation. The apparent p*K* was determined as 6.3 at 44 mM Cl^- (Figure 2c), but this was reduced to 5.5 in the absence of halide ions, in agreement with previous studies (*23*). On the basis of the literature absorption coefficient (ϵ_{514}) of 83 mM^{-1} cm^{-1} for the anionic form, YFP^- (*1*), the ϵ_{390} for the protonated form, YFPH, was determined as 18 mM^{-1} cm^{-1}. The fluorescence emission spectra (excitation at 480 nm) showed a peak at 527 nm that revealed the same p*K* value as the absorption data (Figure 1b, 2c). Excitation at 390 nm yielded an

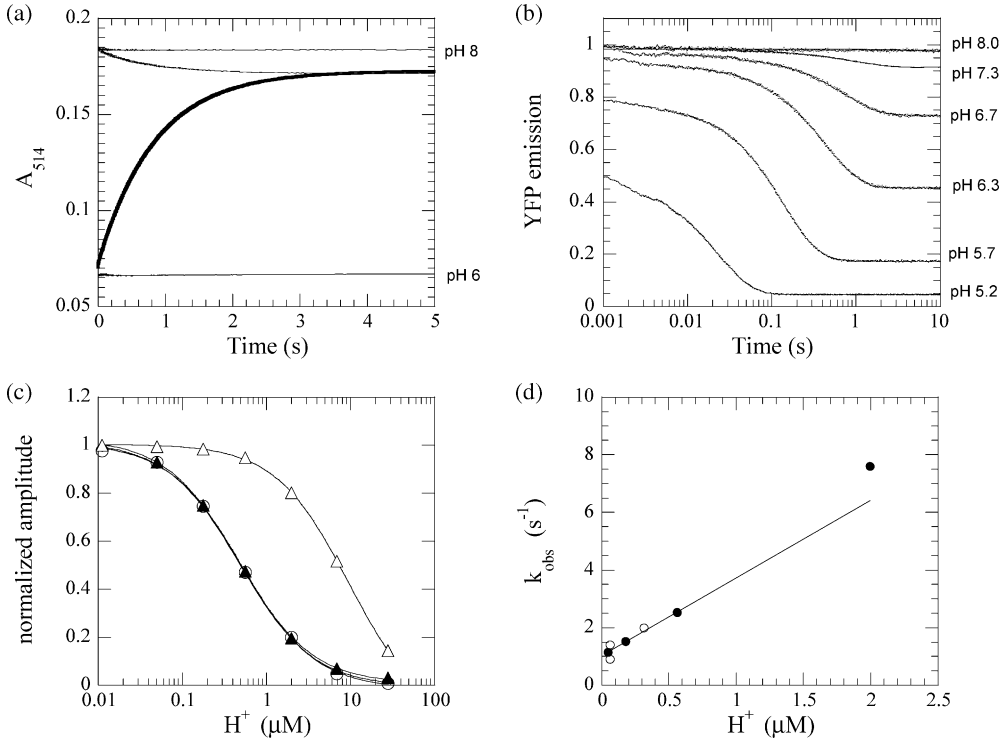

FIGURE 2: The kinetics of YFP protonation. (a) pH-jump absorption stopped flow records monitored at 514 nm (2 mm path length) on mixing 10.5 μM YFP (reaction chamber concentration) in pH 6 buffer (20 mM MES) or pH 8.0 (20 mM TES) with an equal volume of pH 6 or pH 8 buffer at 20 °C. In addition, the buffer contained 40 mM NaCl and 2 mM $MgCl_2$. The pH 6 YFP vs pH 6 buffer (bottom trace) and pH 8 YFP versus pH 8 buffer (top trace) serve to calibrate the initial absorbance values. The pH 6 YFP jump with pH 8 buffer (final pH = 7.3) yielded a single-exponential rise in absorbance with a $k_{obs} = 1.2\ s^{-1}$, while the pH 8 YFP with pH 6 buffer (final pH 7.3) yielded a single-exponential fall in absorbance with a $k_{obs} = 1.4\ s^{-1}$. Note that in the pH 6 to pH 7.3 jump there is a small (≈5% total amplitude) burst phase that is lost within the deadtime of the apparatus. (b) pH-jump fluorescence stopped flow records monitored with 514 nm excitation. 5 μM YFP (reaction chamber concentration) in 40 mM NaCl, 2 mM $MgCl_2$, 5 mM TES at pH 8 was mixed with similar buffers but containing 35 mM MES adjusted to various pH values with acetic acid to give the final pH values indicated. Note that the value of the fluorescence within 1 ms of mixing indicates that an increasing fraction of the signal was lost within the deadtime with decreasing pH. (c) pK determination of YFP. The graph shows three superimposed normalized data sets to yield an overall pK = 6.3 (K_d = 0.51 μM) derived from (i) the A_{514} absorption data of Figure 1a (closed circles), (ii) the emission intensity at 527 nm (open circles) in a similar experiment to that shown in Figure 1b but with the same buffers used in Figures 1a and 2b and (iii) the end-point (10 s) fluorescence values (closed triangles) in the stopped-flow records of Figure 2b. The open triangles correspond to the amplitude observed after 1 ms of mixing and yield a pK = 5.0 (K_d = 9.6 μM). The latter represents the intrinsic pK_{1a} of YFP before the slow isomerization reaction occurs. (d) The observed rate constant (closed circles) for the slow decrease in fluorescence in the records of Figure 2b at pH jumps to 7.3, 6.7, 6.3 and 5.7. The intercept value for a linear fit to the first 3 points yields the rate constant of the reverse isomerization reaction of 1.02 s^{-1}. The gradient of 2.7 $\mu M^{-1}\ s^{-1}$ represents the apparent H^+ association rate constant. Also plotted on this graph (open circles) are the rate constants for the pressure-release transients (Figure 4) obtained at pH 7.2 and 6.5.

Scheme 1

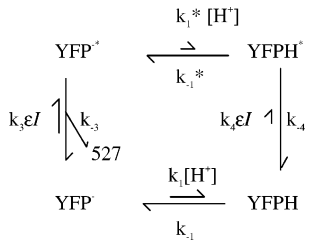

emission signal at 527 nm that was reduced by 125-fold compared with 480 nm excitation (Figure 1c), but no significant emission was detected in the 450 nm to 500 nm region (cf. other YFP variants which show weak emission; (*6*)). Interestingly, the emission intensity at 527 nm with 390 nm excitation was practically independent of pH, indicating that the YFPH species has a reduced quantum yield compared with the YFP^- anion, but this is compensated by an increased absorbance at 390 nm. To explain these observations a basic protonation cycle of YFP is summarized in Scheme 1.

The quantum yield for YFP^- emission, (Φ_{527}), following direct excitation of the anionic species is reported as 0.61 (*1*), from which the quantum yields for emission following YFPH excitation were calculated as 0.022 (Φ_{527}) and <0.002 (Φ_{460}). These data suggest that YFPH* decays by two competing routes: a direct radiationless mode to the YFPH ground state (rate constant k_{-4}) and via an excited-state deprotonation reaction to yield the YFP^{-}* species (rate constant k_{-1}*) which subsequently emits at 527 nm. The relative rate constants for these processes are expected to be about 30:1 respectively, to account for the low fluorescence yield from the YFPH species. These conclusions were tested by direct measurement of the excited-state kinetics, as described below.

Kinetics of the pH induced reaction. To assess the time course of interconversion of the ground-state YFP^- and YFPH species, solutions of YFP were subjected to pH jumps in a stopped-flow spectrophotometer and the change in absorption at 514 nm or emission at >530 nm was monitored. On mixing YFP in pH 6 buffer with pH 8 buffer to give a final pH of 7.3, an increase in absorbance was

Scheme 2

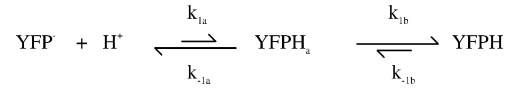

observed with a rate constant of 1.2 s^{-1} and which accounted for 95% of the expected amplitude (Figure 2a). A process with similar kinetics, but with a smaller and inverted amplitude, was obtained when YFP was initially in pH 8 buffer and was rapidly jumped to pH 7.3. The profiles were well fitted by a single exponential and the rate constants were unaffected when the light intensity was reduced 10-fold by closing the excitation slit. The maximum light intensity was estimated as approximately 0.1 mW cm^{-2}, which is several orders of magnitude lower than the laser illumination used in the single molecule measurements described below.

For a 1 step protonation reaction with an apparent p*K* of 6.3 ($1/K_1 = 0.5\ \mu$M), the observed rate constant at pH 7.3 is given by $k_1[H^+] + k_{-1} = 1.2\ s^{-1}$ where $H^+ = 0.05\ \mu$M and thus $k_{-1} = 1.1\ s^{-1}$ and $k_1 = 2.2\ \mu M^{-1}\ s^{-1}$. However, protonation reactions per se are generally very rapid and would be expected to be complete within the deadtime of the stopped-flow apparatus. To assess the presence of a fast phase, the stopped-flow signals were compared with the amplitudes obtained at the starting pH values of 6 and 8 (Figure 2a). In both jump directions there was ≤ 5% loss of signal within the deadtime for the apparatus (1.5 ms) (*24*). To explore this process further, a YFP sample was made up in dilute (5 mM) TES buffer at pH 8.0, where the YFP is 98% ionized, and the pH was jumped to increasingly acid values with a 35 mM MES-acetate buffer (Figure 2b). It was evident that at lower final pH values, an increasing fraction of the signal was lost within the dead time of the apparatus. The final fluorescence value was in accord with that expected from spectral measurements at equilibrium and yielded a p*K* value of 6.3 (Figure 2c). The initial fluorescence value immediately after mixing yielded a pK_{1a} of about 5.0 ($1/K_{1a} = 9.6\ \mu$M). Thus the protonation reaction is clearly a two-step reaction in which a slow isomerization step with equilibrium constant $K_{1b} \approx 19$, pulls over the pK_{1a} to give an apparent p$K = 6.3$. We use the term isomerization here in a general sense. It may involve the protein as a whole and/or a specific change of the chromophore such as a cis−trans isomerization (see Scheme 2, where $YFPH_a$ and YFPH represent low fluorescent protonated isomers). A plot of the observed rate constant for the fluorescence decrease as a function of $[H^+]$ (Figure 2d) is linear over the pH 6 to 8 range and indicates $k_{-1b} = 1.0\ s^{-1}$ from the intercept, while $K_{1a}k_{1b} = 2.7\ \mu M^{-1}\ s^{-1}$, close to the value deduced from the records in Figure 2a for a 1 step scheme above (i.e. apparent $k_1 \equiv K_{1a}k_{1b}$). Thus k_{1b} in Scheme 2 is of the order of 26 s^{-1}. This value cannot be determined exactly because the second step itself has some pH dependence (faster at low pH) and pK_{1a} is also difficult to define because the YFP is unstable at pH values below 5.5. Nevertheless at pH 7.3, where the majority of our studies were performed, the $YFPH_a$ species only represents about 4% of the protonated state and 0.4% of the total YFP and thus the two-step mechanism of Scheme 2 behaves essentially as a one-step reaction (Scheme 1) with an apparent protonation rate constant, $k_1[H^+]$, of about 0.1 s^{-1} and a deprotonation rate constant, k_{-1} of 1.0 s^{-1}, limited by an isomerization of the protonated state.

Although $YFPH_a$ is a minor species, it exists at relatively high concentration transiently when a solution of YFP at pH 8 is rapidly acidified. Time-resolved spectra were recorded using a diode array detector on the stopped-flow apparatus to follow this reaction at a final pH of 5.6 (Figure 3a). Comparison of the spectrum recorded 1.28 ms after mixing with the final endpoint spectrum (10 s) shows that the peak attributed to the protonated species is initially about 420 nm but this shifts to 390 nm during the reaction (Figure 3b). Comparison of the spectrum after 1.28 ms with that of YFP at pH 8.0 shows a 27% reduction in 514 nm absorption that is lost within the deadtime of the apparatus, in agreement with the single wavelength experiment of Figure 2b.

To explore the kinetics of the rapid process further, pressure-jump measurements were carried out in phosphate and imidazole buffers (Figure 4). Phosphate shows a large volume change on ionization (−24 mL mol^{-1} for the mono- to dianion with a p*K* of 7.0; (*14*, *25*)) and thus a pressure-jump in this buffer gives a pH change that acts as an additional perturbation to the system under study. The YFP fluorescence profiles revealed biphasic relaxations in both buffers, with the first phase being practically simultaneous with the pressure change and the second phase having rate constants in the range 0.9 to 1.4 s^{-1} at pH 7.2. The latter values are similar to the rate constant observed by stopped-flow pH-jump kinetics, which are dominated by the value of k_{-1} at this pH (Figure 2d). The amplitude of the overall transient in imidazole buffer (Figure 4b) allowed us to calculate an overall volume change of about +56 mL mol^{-1} for the protonation reaction, from the effect of pressure on $\ln K_1$. The effect of compression was compensated for using a value of 0.046% MPa^{-1} for the compressibility of water. Thus high pressure favors the ionization of YFPH to YFP^-. The amplitude in the phosphate buffer (Figure 4a) was about half that in imidazole buffer which is consistent with a concomitant pH change of −0.023 (for a 5.4 MPa pressure increase) that opposes the ionization reaction. In principle, the amplitude of the fast phase can be analyzed to give the volume change for the ionization of the $YFPH_a$ species. However, the compression of water gives a significant contribution to this phase. Moreover, the uncertainty of the exact value of pK_{1a} introduces a substantial error in this calculation. Pressure-jump measurements at a pH close to pK_{1a}, (i.e. around 5.0) where these problems would be minimized, are complicated by the tendency of the YFP to denature under these conditions. The direct observation of a fast phase at higher pH values does, however, provide independent evidence for a two-step protonation mechanism, as shown in Scheme 2. Furthermore, the increased time-resolution compared with the stopped-flow apparatus, allows more stringent lower limits to be placed on the rate constants for step 1a. Figure 4c shows the pressure release signal and fast YFP response in phosphate buffer at pH 6.5. The lag in the fluorescence response (<20 μs) indicates a lower limit of the relaxation rate constant of $10^5\ s^{-1}$. For a $pK_{1a} = 5$ this indicates that $k_{-1a} \geq 10^5\ s^{-1}$ while $k_{1a} \geq 10^4\ \mu M^{-1}\ s^{-1}$ (Scheme 2).

All of the above transients were measured in the presence of 40 mM NaCl. In the absence of halide ions, the overall p*K* of YFP is reduced to 5.5 (*23*). When equivalent stopped-flow pH jumps were performed in phosphate buffer in the absence of halide ions (see Supporting Information), a similar

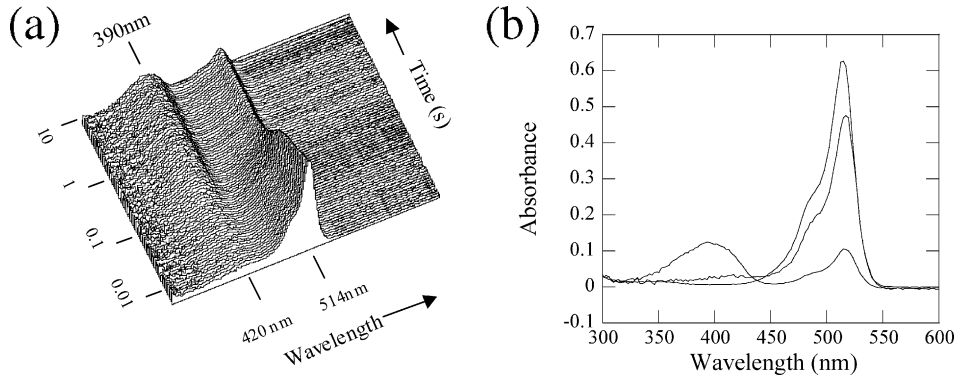

FIGURE 3: Time-resolved absorption spectra for pH jump of YFP (a) spectra on jumping from pH 8.0 to 5.6 using a diode array detector under the conditions used in (Figure 2b) but with 8 μM YFP (reaction chamber concentration, 10 mm path length). (b) Comparison of spectra obtained on mixing YFP at pH 8.0 with pH 8.0 buffer (control) with the same YFP mixed with pH 5.5 buffer to give a final pH of 5.6. Spectra for the latter are shown at 1.28 ms and at the endpoint (7 to 10 s average). Note the loss of 514 nm absorbance in the deadtime, with a concomitant increase in absorbance at 420 nm.

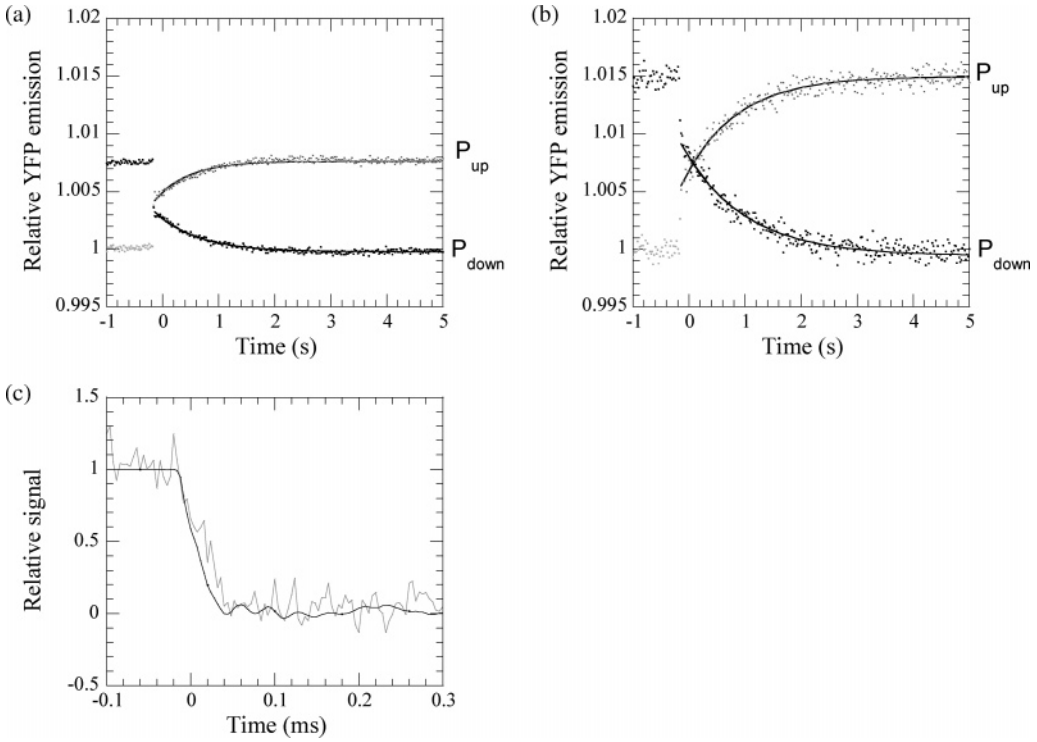

FIGURE 4: Pressure-jump relaxation transients of YFP. (a) 10 μM YFP in 40 mM NaCl, 1 mM $MgCl_2$, 20 mM potassium phosphate at pH 7.2 at 20 °C were subject to 5.4 MPa pressure jumps (gray curve) and releases (black curve). The record shown is an average of 20 repeats taken at 20 s intervals and yields rate constants for the slow phase of 1.8 s^{-1} (pressure up) and 1.4 s^{-1} (pressure down). (b) Similar reaction but in the presence of 20 mM imidazole buffer rather than phosphate. The record shown is an average of 15 repeats taken at 20 s intervals and yields rate constants for the slow phase of 1.0 s^{-1} (pressure up) and 0.9 s^{-1} (pressure down). (c) Normalized signals from the pressure transducer (black) and fluorescence detector (gray) for a pressure release with 10 μM YFP as in (a) but at pH 6.5. The signals are the average of 2400 transients. Records on a longer timebase (not shown) yield a rate constant for the slow phase of 2.0 s^{-1}.

value for the apparent deprotonation rate constant, k_{-1} was found (1 s^{-1}) but the apparent proton association rate constant, k_1 was slowed to 0.3 μM^{-1} s^{-1} (Scheme 1) to account for the lowered p*K*. Thus the slow isomerization reaction is coupled to the protonation reaction per se, and is not simply a reflection of Cl^- binding.

Single Molecule Kinetics. The two-state behavior observed in the absorption spectra (Figure 1a, and ref *22* and *23*), coupled with stopped-flow measurements (Figure 2a) which show the transition between states is slow, require that the fluorescence from a single molecule ($\lambda_{ex} = 514$ nm) exhibits blinking on the seconds time scale due to spontaneous YFP^- to YFPH interconversion. The predicted on- and off-times (*6*) are defined by $1/k_1[H^+]$ and $1/k_{-1}$ respectively, although the on-time with 514 nm excitation will be reduced by photochemical reactions at the laser intensities used in microscopy. To evaluate the blinking rate under our buffer conditions, a YFP-myosin W501+ motor domain fusion protein was immobilized by binding to an actin filament that, in turn, was immobilized on a silica slide and imaged by TIRF microscopy (*11*). In the absence of nucleotide, the YFP-myosin forms a tight bond with actin with a dissociation rate constant <0.01 s^{-1}. At the laser powers used, YFP fluorescence emission was terminated by photobleaching rather than by dissociation from actin. Following photobleaching of a partially decorated filament, single spots were observed corresponding to single YFP-myosin molecules (Figure 5a). These underwent fluctuations in emission

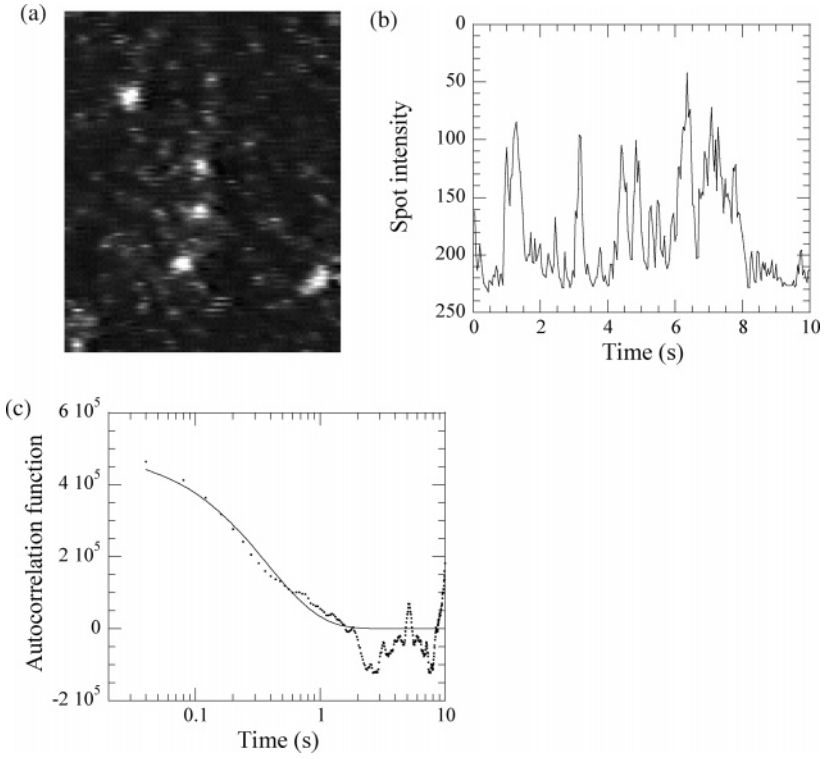

FIGURE 5: Single molecule kinetics. (a) A single video frame of single YFP-myosin molecules bound to an actin filament captured by TIRF microscopy at 2.5 kW cm^{-2} laser intensity. The spots showed blinking behavior for tens of seconds before being bleached (b) Intensity record of one of the spots shown in (a) with a gray scale in which 0 = white and 255 = black. (c) Autocorrelation function of the record shown in (b) with a superposed single-exponential fit of 2.7 s^{-1}. Buffer conditions were 40 mM NaCl, 2 mM $MgCl_2$, 0.1 mM EGTA, 10 mM dithiothreitol, 20 mM HEPES at pH 7.5 and 20 °C.

intensity on the seconds time scale (Figure 5b). Autocorrelation analysis of individual spots yielded decay rates in the range of 2 to 4 s^{-1}, with the total off-time being about twice the on-time during the blinking phase (Figure 5c). For a simple two-state reaction, the decay of the autocorrelation function provides a measure of the sum of the interconversion rate constants, while the ratio of the total on-time to off-time, determined from the average intensity across the profile, provides a measure of the equilibrium constant. These data suggest that at the laser power used (50 mW at the prism entrance, corresponding to a maximum of 2.5 kW cm^{-2} within the evanescent field), the YFP^- emission is prematurely terminated by photoconversion to YFPH, with a rate constant of about 2 s^{-1} (i.e. about 20× faster than the ground-state rate constant), while YFP^- is regenerated from YFPH at the ground-state rate of 1 s^{-1}. These data are very similar to those reported by Dickson et al. (*6*) for a related YFP construct lacking the V68L substitution. At laser powers < 1 kW cm^{-2} fluctuations in emission occur predominantly via the ground state protonation-deprotonation reaction and hence the observed fluctuation rate constant shows only a shallow dependence on laser power in this regime. Dickson et al. (*6*) also noted that between bouts of blinking behavior, single YFP molecules went into a longer-lived dark state, not accounted for by Scheme 1. The mechanism of this photobleaching was investigated further (see below).

Excited-State Dynamics. The emission of 527 nm light, characteristic of the YFP^- anion, when YFPH was excited at 390 nm suggests that YFPH* undergoes a rapid ionization to YFP^{-}*, in an excited-state reaction similar to that previously observed for GFP (*2*). Also, the single-molecule studies described above suggest that intense 514 nm illumination drives the protonation reaction at a rate faster than the ground-state process. To assess the excited-state dynamics of YFP directly, time-resolved fluorescence measurements were made by fluorescence upconversion and TCSPC spectroscopy. Measurements were made at pH 6 with 400 nm illumination to maximize the absorption of the neutral chromophore, YFPH and minimize any underlying high-energy absorption of the anionic species. The time-evolution of fluorescence was probed at two wavelengths, 460 and 525 nm (Figure 6a), close to the emission maxima of the bands observed in the time-resolved emission spectra (Figure 6b). Although no appreciable steady-state fluorescence emission is observed in the 450 to 500 nm range (cf. Figure 1c), the time-resolved emission spectrum at 300 fs showed a prominent peak at 460 nm as well as the 527 nm peak observed in the steady-state spectrum. By 10 ps, the 460 nm peak had decayed away completely and only the 527 nm fluorescence band remained. The fluorescence band at 460 nm is assigned to emission from YFPH* and the fluorescence band at 527 nm is primarily assigned to emission from YFP^{-}*.

The time-resolved fluorescence measured at 460 nm decays away rapidly, with an average lifetime, $\langle\tau\rangle = \sum A_i\tau_i$, of 1.4 ± 0.1 ps. Typically, fits to multiphasic exponentials yielded components with lifetimes about 400 fs (70%) and 2 to 3 ps (25%). The decay of emission monitored at 525 nm, shows an initial rapid decay on the picosecond time scale similar to that observed at 460 nm, followed by a much longer-lived component. The initial rapid decay can be attributed to spectral overlap of the YFPH* and YFP^{-}* emission bands as evidenced in Figure 6b. Under the assumption that the YFPH* is the predominant species

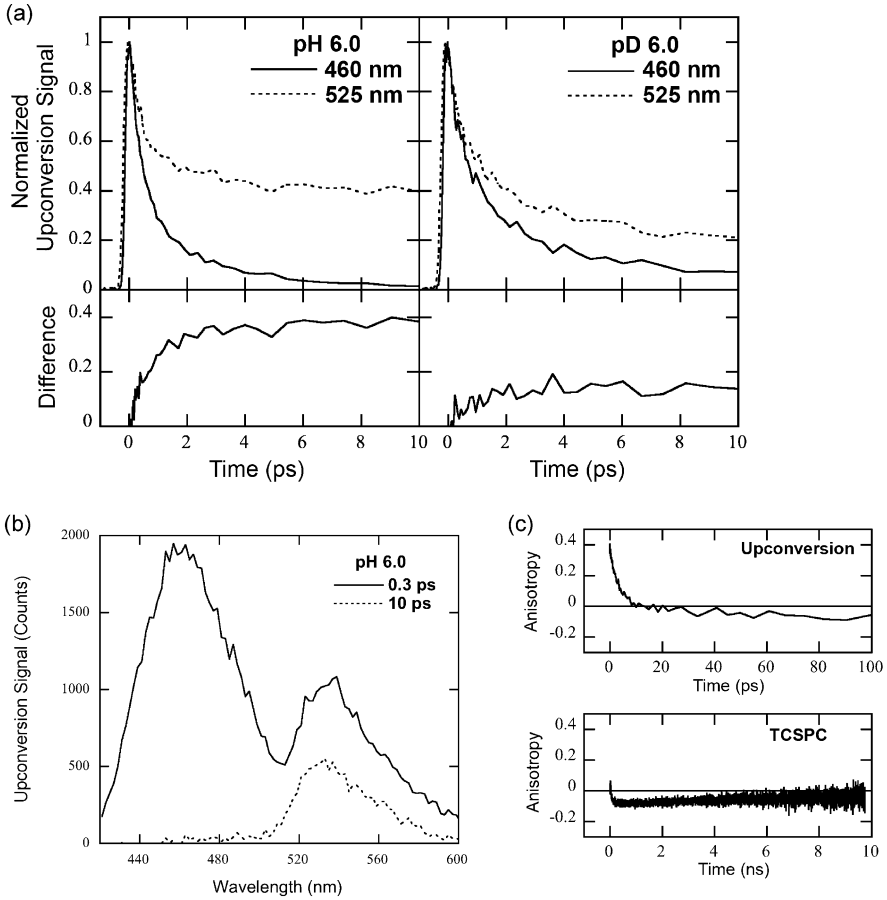

FIGURE 6: Time-resolved fluorescence measurements of YFP following femtosecond excitation at 400 nm. (a) Time-resolved emission of YFP at pH 6 monitored at 460 nm (solid) and 525 nm (dashed). Left panel shows 299 μM YFP in protonated buffer solution; right panel shows 52 μM YFP in deuterated buffer solution. Subtraction of the normalized excited-state emission kinetics at 460 nm from the data measured at 525 nm results in the difference trace shown below each panel and reflects the excited-state dynamics of YFP^{-}*. (b) Time-resolved emission spectra of 493 μM YFP at pH 6. Spectra were acquired at $t = 0.3$ ps (solid) and 10 ps (dashed). (c) Time-resolved anisotropy of 493 μM YFP at pH 6 measured at 525 nm. Upper panel shows the anisotropy acquired by fluorescence upconversion; lower panel shows the anisotropy acquired by TCSPC.

directly excited at 400 nm, the "instantaneous" (IRF-limited) emission at zero time should arise entirely from the low-energy side of the YFPH* emission band. Normalization and subtraction of the YFPH* kinetics measured at 460 nm to time-resolved fluorescence measured at 525 nm results in a difference trace that reflects the excited-state dynamics of YFP^{-}*, shown in the lower panels of Figure 6a. YFP^{-}* is observed to rise on a time scale comparable to the decay of YFPH* and subsequently decay on a much longer time scale. The long-time decay of YFP^{-}* emission at 525 nm was determined to be 3.5 $\pm$ 0.3 ns by TCSPC (cf. Figure 7b for an equivalent experiment done at pH 8.0 where the time constant was 3.2 ns). The integral of this curve accounts for the domination of the 525 nm emission in the steady-state spectrum (cf. Figure 1c). To ascertain the dominant mechanism of decay from YFPH*, analogous measurements were made after exchanging the protein into deuterated buffer. The average lifetime of YFPD* emission, as measured at 460 nm, was observed to increase slightly to 2.2 $\pm$ 0.2 ps. The difference between the excited-state dynamics measured at 460 and 525 nm is smaller in deuterated buffer, indicating that the contribution of fluorescence from YFP^{-}* at that wavelength had decreased (see difference trace in Figure 6a). The long-time decay of YFP^{-}* was unaffected by deuteration and remained 3.5 ns. These results provide confirmation of the conclusion from the steady-state data (Scheme 1) which indicated that YFPH* decays predominantly via a radiationless route (k_{-4}) while a small but significant fraction undergoes ionization to YFP^{-}* (k_{-1}*). The deuterium isotope effect reduces k_{-1}, which has a minor effect on the observed rate constant ($k_{-4} + k_{-1}$*), compared with equivalent observations on GFP (*2*), but a larger effect on the amplitude of YFP^{-}* emission.

The time-resolved anisotropy of YFP was also examined by fluorescence upconversion and TCSPC. Following excitation at 400 nm at pH 6, the time-resolved anisotropy measured at 460 nm by upconversion is constant over the short lifetime of YFPH*, exhibiting an average anisotropy of 0.38 $\pm$ 0.03 (data not shown). In contrast, the time-resolved anisotropy measured at 525 nm by fluorescence upconversion (Figure 6c, upper panel) shows a rapid decrease from an initial value of 0.39 to -0.10 with time constants of 3.2 $\pm$ 0.2 ps (74%) and 68 $\pm$ 14 ps (26%). Monitoring the time-resolved anisotropy by TCSPC shows a similar rapid decrease in anisotropy approaching -0.10 on the picosecond time scale, although the time-resolution is not adequate to fully resolve the initial decay (Figure 6c, lower panel). The anisotropy then approaches zero on the nanosecond time scale, presumably with the rotational lifetime of YFP. It is important to note that control experiments on S65T GFP at pH 6 produced anisotropy results in agreement with those reported previously (*26*) and that a solution of coumarin-

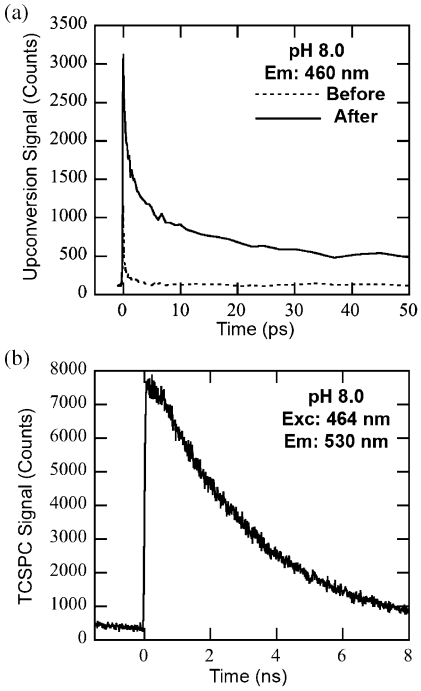

FIGURE 7: Time-resolved emission spectra. (a) 425 μM YFP at pH 8 before (dashed) and after (solid) photoconversion by exposure to 532 nm pulses from a Nd:YAG laser for 1 h. (b) Time-resolved emission of 1.8 μM YFP at pH 8 monitored at 530 nm following excitation at 464 nm. Fitting to a single exponential yielded a lifetime of 3.2 ns.

480, a freely rotating laser dye, exhibited a uniformly zero anisotropy following rotational depolarization indicating no significant instrumental bias of the parallel or perpendicular signals.

YFP Photobleaching. We previously noted that UV light from a Xe flash lamp partially regenerated the fluorescence from YFP molecules that had been bleached by irradiation with 514 nm light (*11*). This finding was also reported by Miyawaki and Tsien (*10*) who showed that light between 330 and 390 nm was effective for photoactivation, while Dickson et al. (*6*) achieved switching at 405 nm (with a slightly different YFP construct). The YFP^- anion shows very weak absorption in this region (Figure 1a). We therefore surmised that the dark state induced by prolonged photobleaching of YFP^- with 514 nm light might develop a new absorption band in the near UV to account for its photochromic properties. A YFP solution at pH 7.2 was therefore irradiated with a 250 mW 514 nm laser beam in a microcuvette and the absorption spectrum was monitored. After 10 min irradiation, with intermittent stirring, the 514 nm absorption peak was reduced by 80% and a new weak absorption band appeared in the UV region which peaked at 390 nm (Figure 8a, b). Complete photobleaching was difficult to obtain because the laser beam was narrower than the sample volume and mixing during illumination may not be complete. However, the spectrum of the 100% photobleached sample could be estimated by subtraction of an appropriate fraction of the starting YFP spectrum, assuming the product had no discrete peak at 514 nm. This procedure indicated the photobleached product(s) also had a weak absorption peak at 470 nm, as well as that at 390 nm which was observed directly. The time course of photobleaching yielded an isobestic point at 454 nm (Figure 8a), suggesting a simple precursor-product relationship. However an isobestic point would still be obtained if two or more products were formed with distinct spectral properties, but in a constant product ratio. This seems a likely possibility because the limited recovery on photoactivation (see below) suggests that photobleaching yields an irreversibly bleached product (denoted XFP which may itself represent several states) and a reversibly bleached product (denoted YFPHrb).

The changes observed in the absorption spectrum of YFP during photobleaching did not depend significantly on the excitation source (CW 514 nm, CW 532 nm, pulsed 532 nm). Excitation at either 514 or 532 nm in CW mode was followed by the slow, spontaneous, partial recovery of 514 nm absorption band when the sample was kept in the dark (see below). The mass spectra of these samples showed no change in mass after photoconversion. Excitation with pulsed 532 nm light, however, showed little or no sign of recovery ($\leq$2%) after photobleaching even over the course of $\sim$ 10 h. The mass spectrum after photoconversion showed the appearance of a new peak 44 $\pm$ 2 Da lower than the YFP peak at 29 004 Da (Figure 9) consistent with the loss of CO_2 from the protein. Clearly, this change is irreversible and the product contributes to the XFP state. Previous studies showed that E222 is prone to decarboxylation (*27*). In an attempt to test this idea we made an E222A YFP mutant. This construct showed no absorption or fluorescence in the visible region, but the tryptophan emission and the far UV circular dichroism spectra (*28*), indicated the protein was folded into a native state. However the mass spectrum yielded 28 964 rather than the expected 28 946 for the E to A substitution. This suggests that the final dehydration step in chromophore maturation had not taken place. Thus, the lack of 527 nm emission did not prove that E222 is required to favor the strongly emitting fluorescence YFP^-state.

From the analysis of the recovery of fluorescence, it appears that the 390 nm peak observed on photobleaching arises predominantly from XFP species (see below). The excited-state dynamics of this species was examined by irradiating samples of YFP at pH 8 at 532 nm with an Nd:YAG laser for 1 h. Measurements were made at pH 8 to minimize the contribution of YFPH absorption in the near UV Photoconversion of the sample resulted in changes in the absorption and emission spectra analogous to that observed by CW argon ion laser irradiation (Figure 8a), although the rate of photoconversion was slower due to the relatively poor overlap of the 532 nm laser light with the YFP^- absorption band. As described earlier, these samples formed from pulsed 532 nm excitation exhibited little or no spontaneous recovery of the 514 nm absorption band and the mass spectra showed a new peak 44 Da lower than the YFP peak (Figure 9). Following excitation at 400 nm, samples of photoconverted YFP showed a dramatic increase in the magnitude and lifetime of 460 nm emission compared with control samples not exposed to laser light (Figure 7a cf. 6a). The average lifetime $\langle\tau\rangle$ observed for YFPHrb* was 49 $\pm$ 4 ps. The decay of emission monitored at 525 nm in the photoconverted sample showed a decrease in the longest measured time constant, 4.3 $\pm$ 0.2 ns, compared with the 5.1 $\pm$ 0.1 ns decay of emission observed for the control YFP sample at pH 8. However, these measurements are distorted by reabsorption of emitted photons owing to the high fluorophore concentration (*29*). At low concentrations (<2

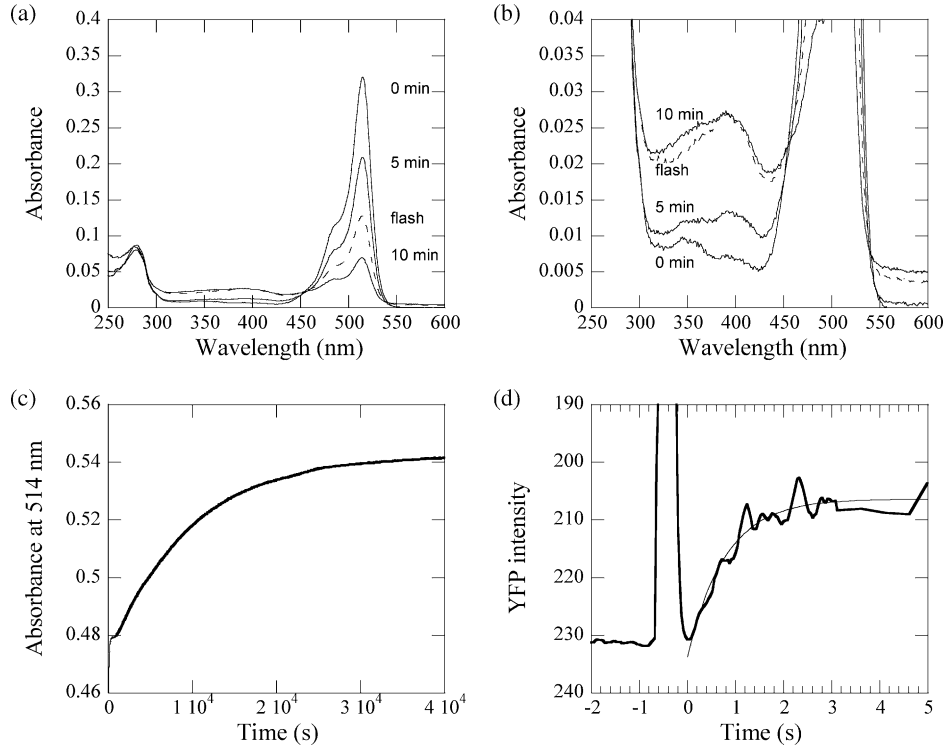

FIGURE 8: Photobleaching and photoactivation of YFP. (a) Absorption spectra YFP (4.7 μM) in a 10 mm path length microcell before and after 5 and 10 min exposure to 250 mW of 514 nm laser light (solid lines with decreasing absorbance at 514 nm). The sample was then subjected to a Xe flash (280 to 380 nm) to cause partial recovery in absorbance at 514 nm (dashed line). A second flash caused no further change. (b) The same spectra magnified to show recovery in the 300 to 400 nm region. (c) Spontaneous recovery of the absorbance at 514 nm over 11 h by a bleached sample maintained in the dark (apart from weak 514 nm probing light applied for 1 s every minute). The superposed fit to a single exponential corresponds to a rate constant of 1.0×10^{-4} s^{-1}. (d) Photoactivation of bleached YFP-myosin molecules bound to an actin filament by a Xe flash derived from the data shown in Figure 10. Superposed fit yields a rate constant of 1.3 s^{-1}.

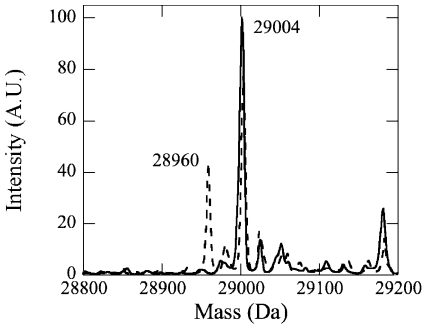

FIGURE 9: Mass spectra of YFP (solid) and YFP photobleached at pH 8 for 1.5 h (dashed). The intensity is normalized to the parent peak for each spectrum. Photobleaching produced a secondary peak at 44 Da lower than the parent peak at 29 004 Da.

μM) the lifetime of the YFP$^-$ emission was 3.2 ns (Figure 7b), in line with previous estimates (*4*). Polarized TCSPC experiments at pH 8 after photoconversion showed essentially identical time-resolved anisotropy dynamics at 525 nm as those observed for untreated YFP at pH 6 (data not shown).

Photoactivation of Bleached State. After 80% photobleaching with CW 514 nm light, the YFP sample shown in Figure 8a was subject to a 4 ms flash from a Xe flash lamp focused to almost fully illuminate the sample in the microcuvette with 280 to 380 nm light. The absorbance at 514 nm showed an immediate (i.e. within the 1 min required to transfer the sample to the spectrophotometer) but incomplete recovery (Figure 8a dashed line). A second flash contributed little to the total observed recovery, which amounted to 24% reversal of the 80% reduction in the absorbance at 514 nm achieved by photobleaching. By using different filters in front of the Xe flash lamp, a crude action spectrum was determined. Photoactivation was achieved with a 320−390 nm band-pass (Omega 365HT25 DAPI excitation filter), but light above 395 nm was ineffective. Photoactivation was accompanied by a reduction in the near UV absorbance, as expected, but this was not coincident with the 390 nm peak, but rather at 340 and 430 nm (Figure 8b).

If the photobleached sample was kept in the dark, apart from a 1 s exposure every 1 min to weak pulsed Xe light source at 514 nm light in the spectrophotometer, the absorbance recovered spontaneously over a period of several hours (Figure 8c). The main phase of recovery occurred with a rate constant of 1×10^{-4} s^{-1} to a value that corresponded to 28% of the initial bleach. Subjecting the dark-recovered sample to a Xe flash produced no further change. Thus it appears the species that is activated by the Xe flash is the same as that which shows spontaneous recovery in the dark. When the sample was treated to a second round of photobleaching by 514 nm light from the laser and then activated with a Xe lamp, a 25% recovery was again observed i.e., 6% relative to the initial intensity. This suggests that during photobleaching, two product pools are formed in an approximately constant ratio of about 3:1. The dominant species is an irreversibly bleached species (denoted XFP), while the reversibly bleached (dark) species (YFPHrb) amounts to about 25% of the initial YFP concentration. The partition ratio is not an exact constant because the YFPHrb species will slowly reactivate and eventually the whole sample will become XFP on prolonged irradiation. Therefore the longer

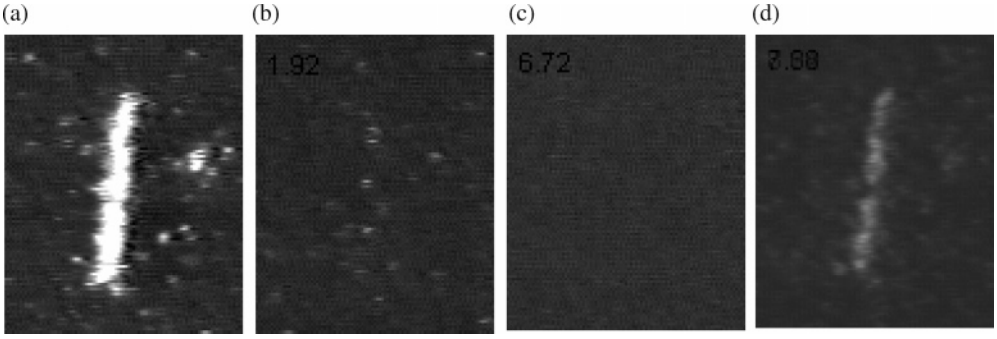

FIGURE 10: Photobleaching and photoactivation of YFP-myosin bound to an actin filament. (a) TIRF microscope image of decorated filament when first illuminated at 0.25 kW cm^{-2} laser intensity. (b) After bleaching at 2.5 kW cm^{-2} intensity and return to 0.25 kW cm^{-2} laser intensity. (c) 80 ms after Xe flash. (d) 2 s after Xe fash. The photoactivation time course is analyzed in Figure 8d. Buffer conditions were as in Figure 5.

the sample is bleached with 514 nm light, the less the yield of photorecovery. Miyawaki and Tsien (*10*) reported a 21% yield after photoactivation with continuous irradiation with UV light (330 to 390 nm). The intensity of the light they used was much lower than the Xe flash lamp used here and the recovery occurred with a half-time of around 500s (i.e. an order of magnitude faster than the spontaneous recovery that we found in the dark, Figure 8c).

The spontaneous recovery in the 514 nm peak was accompanied by no detectable decrease in the 390 nm peak. Rather there was some loss in absorbance at 430 nm but very little change was observed at 350 nm (cf. with Xe flash activation). It is possible that the decrease in 350 nm absorbance on flashing is due to photobleaching by the flash lamp itself. On the other hand, light in the region of 350 nm is effective in photoactivation, whereas light at 430 nm is not. These findings lead to the conclusion that the YFPHrb species absorbs very weakly at 350 nm so that its contribution is swamped by the 390 nm absorbance of XFP, but it is sufficient to allow activation by 350 nm light. On the other hand, the 430 nm absorption band of this product, which is detectable in the difference spectrum before and after spontaneous 514 nm recovery in the dark, does not lead to photoactivation. It is possible that the 430 nm band is associated with the ionized form, YFP^{-}rb, but excitation of this species does not lead to rapid conversion (sub-ns) to YFPHrb* and hence there is no efficient route back to YFP other than the slow, spontaneous pathway.

To measure the actual rate of photoactivation, the activating flash and subsequent monitoring of kinetics must be performed in the same apparatus. This was readily achieved in our TIRF microscope (*18*) using YFP-myosin decorated actin filaments as a sample. Figure 10a shows such a filament recorded immediately after illumination with 514 nm laser beam (5 mW at the prism; 0.25 kW cm^{-2} in the evanescent field). Under these conditions the YFP fluorescence was observed to bleach with a rate constant of 0.055 s^{-1}. Increasing the laser power up to 50 mW at the prism caused further photobleaching at 0.30 s^{-1}. At this point the filament was no longer observed to be continuously labeled but single molecules were observed to undergo bouts of blinking, as shown in Figure 5a,b. Reducing the laser power back to 5 mW gave a very weak image (Figure 10b). When subject to a Xe flash, YFP fluorescence recovery was not immediate (Figure 10c) but the filament image returned over a period of about 2 s (Figure 10d) before being slowly photobleached again with a rate constant of approximately 0.05 s^{-1}. Analysis of the recovery kinetics yielded a rate constant for photoactivation of 1.3 s^{-1} (Figure 8d) while the extent of recovery relative to the initial filament intensity (Figure 10a) was about 20%. The rate constant of recovery is very close to the rate constant determined for the YFPH to YFP^{-} equilibration at pH 7.3 (Figure 2a). It therefore appears that upon UV irradiation YFPHrb is excited to YFPHrb* which then coverts to YFPH*. As indicated by the spectra in Figure 1c, YFPH* returns to the ground state about 30 times faster than the excited-state deprotonation event that yields YFP*. Thus the immediate product after the flash is predominantly YFPH, which then reequilibrates to give the fluorescent YFP^{-} species with a rate constant close to that measured in the pH-jump and pressure-jump experiments (1.2 s^{-1} at pH 7.3) at low laser powers (0.25 kW cm^{-2}). When the experiment was performed under continuous 514 nm TIRF illumination at 2.5 kW cm^{-2}, the same phenomenon was observed, however the photoactivation rate constant was 4.8 s^{-1} and subsequent photobleaching was 0.31 s^{-1}. This is consistent with photoactivation occurring via the YFPH ground-state intermediate, however the reequilibration to YFP^{-}, following the activating Xe flash has a dominant contribution through the excited-state pathway driven by 514 nm illumination (i.e. the photoactivation rate constant is similar to the blinking rate constant (Figure 5c) monitored at the same laser power).

DISCUSSION

The complex photophysics of the GFP family of proteins is a well-recognized problem that needs to be understood for their optimal applications in biology. The YFP class, in particular, exhibit the phenomenon of emission blinking on the seconds time scale, as well as a long-lived low fluorescence state that can be activated by near UV irradiation. Previous studies of GFP and related proteins have identified at least 3 ground-state species and have suggested interconversions between them that give rise to blinking and switching behavior (*2*, *3*, *6*−*9*). However the ground-state kinetics have not been fully rationalized in a manner that is consistent with the observed p*K* values. We propose a revised scheme that relates protonation and photobleached states as shown in Scheme 3.

The core cycle of this mechanism involves the ground-state (YFP^{-} ↔ YFPH) and excited-state (YFP^{-}* ↔ YFPH*) protonation reactions, as defined by Scheme 1. In Scheme 3, XFP represents a photobleached pool that accumulates

Scheme 3

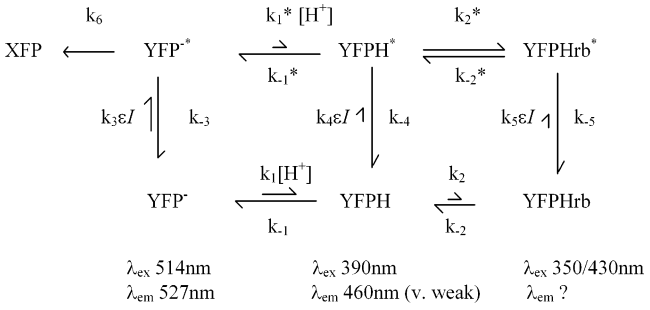

through an effectively irreversible step (k_6). However this product(s) itself shows weak fluorescence and is considered further in Scheme 4 below. Using pH jump stopped-flow methods (Figure 2) we show that blinking in 527 nm emission arises from an isomerization that is coupled to the protonation of the highly fluorescent YFP^- anionic state (i.e. step 1). Blinking is thus a consequence of a ground-state reaction (i.e. the dominant protonated state, YFPH, does not absorb significantly at the excitation wavelength of 514 nm). At pH 7.2, the effective rate constants $k_1[H^+] = 0.2\ s^{-1}$ and $k_{-1} = 1\ s^{-1}$ are defined by the ground-state pK and the observed rate of interconversion in a pH jump experiment. The intermittent dark state can therefore be attributed to the 17% YFPH that exists under these conditions. These parameters account for the blinking reaction at the single molecule level (Figure 5 and ref *6*). This explanation differs from the quantum mechanical calculations of Weber et al. (*30*) who proposed that blinking resulted from the rapid radiationless decay of an excited zwitterionic state. Nevertheless we show here (Figure 6) that the protonated YFPH* state (neutral and/or zwitterion) does, indeed, have a very short lifetime. The radiationless decay route dominates over both 460 nm emission and the excited-state proton dissociation to yield YFP^-*. In the latter respect GFP differs from YFP, where the deuterons had a marked effect on the rate constant of the upconversion event of GFP, showing proton transfer (k_{-1}*) was the dominant process contributing to the observed kinetics (k_{-1}* + k_{-4}) (*2*). In contrast, in the case of YFP, deuterons mainly affected the amplitude of the upconversion process, showing that k_{-4} dominated the rate term (Figure 6a). These results are consistent with the steady-state properties of YFPH which showed very weak emission at 527 nm compared with the YFP^- anion and no measurable emission at 460 nm. The latter can only be detected within the first 2 ps following ultrafast excitation.

The stopped-flow studies also revealed that the ground-state protonation reaction is a two-step process. The initial protonation step has a pK_{1a} of about 5, but a subsequent slow isomerization has an equilibrium constant $K_{1b} \approx 19$, to yield an overall pK = 6.3; the value observed in equilibrium titrations in 44 mM Cl^- , from the absorbance at 514 nm or emission at 527 nm. At pH 7.2 the initial $YFPH_a$ species is a minor component (Scheme 2) and hence it is omitted from Scheme 3 for simplicity. $YFPH_a$ was characterized by rapidly jumping the pH from 8.0 to 5.5 to reveal its maximum absorbance at about 420 nm, compared with 390 nm for the final YFPH state. The kinetics of step 1a (Scheme 2) are too fast to measure by rapid-mixing and, indeed, are at the limit of pressure-jump relaxation measurements. From the latter we estimate $k_{-1a} \geq 10^5\ s^{-1}$ and $k_{1a} \geq 10^{10}\ M^{-1}\ s^{-1}$.

Relatively few transient kinetic studies have been carried out to investigate GFP protonation reactions. Previous pH jump studies with YFP proteins yielded observed rate constants of about 100 s^{-1} at pH 7 for the YFP−H148Q mutant, but this was reduced to 7 s^{-1}, in the presence of Cl^- ions (*31*). In the case of eGFP (S65T), most of the expected amplitude was too fast to measure (>1000 s^{-1}) when the pH was rapidly perturbed in a stopped-flow apparatus (*32*), but a transient was observed with a rate constant of 11 000 s^{-1} when induced by laser flash photolysis of caged protons (*33*). In our ionic conditions, we found there was a small residual biphasic signal with eGFP on a pH jump to 7.2 with rate constants of 230 s^{-1} and 18 s^{-1}. The latter could account for the single-molecule blinking of eGFP that was just resolved at video acquisition rate (*34*, *35*). Overall these data provide a self-consistent explanation as to why blinking on the seconds time scale with eGFP is much less evident than with YFP. It appears the initial protonation step (K_{1a}, Scheme 2) is similar for eGFP and YFP, but that the isomerization is slower and K_{1b} larger for YFP. It is the second step that results in the increased net pK for this variant.

The fluorescence lifetime and quantum yield of YFP (i.e. the predominant species YFP^-) have been determined as 3.7 ns and 0.61 respectively (*1*, *4*). We confirmed this lifetime under our experimental conditions (Figure 7b). YFP^- therefore decays back to the ground state with a rate constant k_{-3} of about $3 \times 10^8\ s^{-1}$, and a radiative component of $2 \times 10^8\ s^{-1}$ (Scheme 3). The effective value for the excitation rate constant $k_3\epsilon I$ depends on the light intensity, I, and the absorption coefficient, ϵ, at the particular wavelength. An estimate of $k_3\epsilon I$ at a particular laser power can be made as follows. YFP^-* is the predominant excited-state species under these conditions and therefore controls the net photobleaching rate. The rate of XFP production (the predominant photobleached species) therefore reflects the concentration of YFP^-*. It has been estimated that YFP has a quantum

Scheme 4

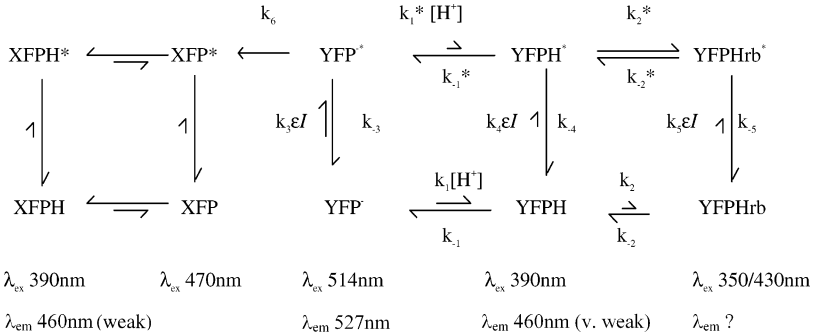

yield for photobleaching of about 8×10^{-6} and therefore each molecule will emit on average about 10^5 photons (*5*, *9*). The ratio of the quantum yield for fluorescence and quantum yield for photobleaching together with the fluorescence lifetime, defines the value of k_6 to be about 2000 s^{-1}. At low laser powers, when $K_3\epsilon I \ll 1$, the observed rate of photobleaching is approximately defined as $K_3\epsilon I k_6$. Thus, at 0.25 kW cm^{-2}, the observed photobleaching rate of 0.055 s^{-1} indicates $K_3\epsilon I = 3 \times 10^{-5}$, and hence $k_3\epsilon I = 6 \times 10^3$ s^{-1}. At 514 nm the relative absorption coefficients of YFP^- and YFPH indicate that $k_3\epsilon/(k_4\epsilon) \geq 50$ and hence $k_4\epsilon I \leq 120$ s^{-1} at this laser power. At all laser powers used in this study, $K_3 \ll 1$ and therefore the system is well below saturation of both the singlet and potential triplet state. The latter may become significant in confocal microscopy and contribute to flickering on the 1 μs time scale in FCS experiments at laser intensities above 100 kW cm-^{2} (*4*).

The low quantum yield of 527 nm emission ($\phi_{527} = 0.022$) when YFPH is excited at 390 nm suggests that the ratio of the rate constants $k_{-4}/k_{-1}^* = 30$. This deduction assumes that $k_{-1}^* \gg k_1^*[H^+]$ at pH 7.2, which seems reasonable (see below). The lack of deuterium isotope effect on the observed excited-state proton-transfer rate constant provides direct evidence that $k_{-4} > k_{-1}^*$, and provides an estimate of k_{-4} of about 7×10^{11} s^{-1}. Consequently, we estimate $k_{-1}^* = 2 \times 10^{10}$ s^{-1}. Thus, as with GFP (*2*), excitation of YFPH leads to rapid proton dissociation, but the yield of this reaction is much reduced by competition with the radiationless return to the YFPH ground state.

The mechanism of Scheme 1 predicts a nonlinear photobleaching rate because at laser powers greater than 0.25 kW cm^{-2}, the absorption of 514 nm light by YFP^- will drive the protonation reaction via the excited-state pathway $YFP^- \rightarrow YFP^{-*} \rightarrow YFPH^* \rightarrow YFPH$ at a rate faster than the ground-state process (0.2 s^{-1} at pH 7.2) and will result in the build-up of YFPH above its dark equilibrium concentration (i.e. dark fractional occupancy of 0.17). This will make the increase in the concentration of YFP^{-*} nonlinear with light intensity, even at light levels well below any putative triplet-state saturation (*4*). This excited-state route accounts for the weak dependence of the blinking rate on laser powers used in the range of 0.1 kW cm^{-2} to 5 kW cm^{-2} (*6*, *9*). At lower laser powers the observed blinking rate is dominated by ground-state protonation and hence is independent of laser power. As the laser power is increased, the on-times, reflecting the lifetime of the YFP^- state become truncated by photoconversion to YFPH, while the off-times are less effected by 514 nm light and are dominated by the dark rate constant k_{-1} of 1 s^{-1}. If it is assumed that YFPH absorption at 514 nm is negligible (i.e. $k_4\epsilon I = 0$), then the flux around photon-driven protonation cycle (Scheme 1) can be solved in the steady-state, at any given light intensity by standard kinetic methods (*36*, *37*). This leads to the solution defined by eq 1 (see Supporting Information).

$$\frac{v}{[YFP]_0} = \frac{I}{\frac{1}{K_3\epsilon K_1^*[H^+]k_{-4}} + \frac{1}{K_3\epsilon k_1^*[H+]} + \frac{K_1}{K_3\epsilon k_1^*} + \frac{I}{k_{-1}}} \quad (1)$$

From such an analysis, the value of $k_1^*[H^+]$ at pH 7.2 must be of the order of 10^4 s^{-1} to account for our data. The value of $k_1^*[H^+]$ compared with the photobleaching rate constant k_6 suggests that YFP will blink, on average, about 5 times before being bleached. This number is consistent with experimental data (*6*). The excited-state p*K* derived from $k_1^*[H^+]$ and k_{-1}^* is therefore deduced to be about 1 compared to 6.3 in the ground state. With 514 nm light at a power of 2.5 kW cm^{-2} and with $k_1^*[H^+] = 10^4$ s^{-1}, the steady-state solution gives fractional occupancies of YFP^- (0.24), YFP^{-*} (7×10^{-5}), YFPH* (7×10^{-12}), YFPH (0.75) compared with the dark distribution of YFP^- (0.89), YFPH (0.11). The calculation is not very sensitive to the absolute values of k_{-1}^* and k_{-4} but-to-their ratio, which is better defined by experiment. The effective conversion rate of YFP^- to YFPH is increased from 0.2 s^{-1} to 3 s^{-1} (see Supporting Information), in line with the observed blinking rate constant (Figure 5c) and photoactivation rate constant (4.8 s^{-1}) at this laser power. It is likely that the absorbance of YFPH at 514 nm although weak, is not negligible and high laser powers would also drive the deprotonation reaction as well, such that the overall conversion rate from YFPH to YFP^- exceeds its ground-state value of 1 s^{-1}.

In addition to the protonation cyle, there are two photobleaching pathways, one of which leads irreversibly to the XFP product(s) and accounts for around 75% of the flux (Scheme 3). The rate constant (k_2^*) controlling the other route to the long-lived reversibly bleached state (YFPHrb) therefore has to be defined to achieve 25% of the flux i.e., $K_1^*[H^+]$-$k_2^* = k_6/3$, when $K_1^*[H^+] \ll 1$, and hence $k_2^* = 2 \times 10^8$ s^{-1}. Thus photoactivation gives a recovery of about 25% of the initial [YFP]. The value of K_2^* is not well defined but is probably close to unity. Unfortunately, the properties of YFPHrb are difficult to define because the near UV absorbance and probably the weak emission at 460 nm (Figures 1d and 6d) are dominated by the XFP species. It appears YFPHrb has weak absorption bands at 350 and 430 nm. It is likely that YFPHrb* decays rapidly by a predominantly radiationless process with $k_{-5} \gg k_{-2}^*$, so trapping the species in a long-lived non- or weakly fluorescence state. In the dark YFPHrb reverts slowly back to YFPH and YFP^- limited by $k_{-2} = 1 \times 10^{-4}$ s^{-1}. This reaction is spontaneous in the direction of YFPH (and hence YFP). Fresh YFP samples stored in the dark show no increase in fluorescence when flashed with UV light. This suggests $K_2 \leq 0.1$ and $k_2 \leq 10^{-5}$ s^{-1}, and hence YFPHrb only builds up after 514 nm illumination. YFPHrb shows, at most, only weak absorption at 514 nm ($k_5\epsilon \leq 0.04k_3\epsilon$), but this might be sufficient to cause slow photoactivation of YFPHrb back into the main photocycle and ultimately yield XFP. However with 350 nm illumination, $k_5\epsilon \geq k_3\epsilon$ leading to significant flux (photoactivation) of YFPHrb via the intermediates $YFPHrb^* \rightarrow YFPH^* \rightarrow YFPH \rightarrow YFP$ which is limited by the last step (k_{-1}) at 1 s^{-1}. The observation of a process at about 1 s^{-1} on photoctivation (Figure 8d) provides indirect evidence that YFPHrb is a protonated species.

In Scheme 3, XFP is introduced as a sink containing "irreversibly bleached" YFP species. However, it is likely to comprise a mixture of states, some of which show weak emission. The peak absorption at 390 nm (Figure 8b) suggests that the dominant XFP state is protonated. It is distinct from YFPH in that femtosecond excitation of XFP leads an intermediate with a longer lifetime to yield XFP^-

(Figure 7a) and weak 460 nm emission can be detected in the steady-state fluorescence spectrum (Figure 1d). The extent of XFP emission at longer wavelengths cannot be easily determined as it is dominated by residual unbleached YFP^-. However, there are indications from difference spectra that XFP (the anion?) absorbs around 470 nm. Scheme 3 can therefore be extended to include the protonation cycle of XFP (Scheme 4).

The nature and kinetics of this cycle are not well defined, other than it appears that the ground-state p*K* is >7 and XFPH is favored. It is possible that XFPH* can also be formed directly from YFPH*, but this reaction would also have to be effectively irreversible to maintain thermodynamic balance. We noted that photobleached samples tended to become turbid, particularly at pH < 7, suggesting the protein was denaturing and aggregating. The gradual rise in the apparent UV absorbance made it difficult to detect small spectral shifts associated with photoactivation (e.g. Figure 8b). Complete or partial unfolding of the protein may, in itself, account for the production of XFP. In so far as comparisons can be made, XFP has spectroscopic properties similar to the free hydroxybenzylideneimidazolidinone chromophore, which has a p*K* of 7.9 with absorption peaks at 390 nm (protonated) and 450 nm (ionized), and is practically nonfluorescent at room temperature (*38*, *39*). Finally, we found that laser light delivered in nanosecond pulses tended to decarboxylate the YFP. This would constitute an irreversible modification, but it cannot explain the XFP species generated during photobleaching with a CW laser.

These studies and conclusions are broadly in line with previous literature, although the variety of GFP mutants studied and variable ionic conditions make direct comparisons difficult. In general, our data support the conclusions of Dickson et al. (*6*) regarding the origin of the blinking and switching phenomena exhibited by the YFP class. In the notation of their scheme $YFP^- = A$, YFPH = I and YFPHrb = N. Our data suggest however that direct decay of N* to A on photoactivation does not occur, but leads to I* and then I as a dark state intermediate. Although Dickson et al. (*6*) suggested A and I states were related by protonation state, as we propose, this conclusion was questioned by Peterman et al. (*9*) who found the blinking rates on the millisecond to seconds time scale were insensitive to pH over the range of 6 to 10. However the latter study focused on GFP variants with lower p*K* values and laser powers were used up to 5 kW cm^{-2}, as a result the on-times were much shorter than those reported by Dickson et al. (*6*) and approached the temporal resolution limit of their imaging device.

We compare our interpretation of the results further in the Supporting Information, with reference to fluorescence correlation spectroscopy (FCS) of Schwille et al. (*4*), low-temperature absorption spectroscopy of Creemers et al. (*3*) and single-molecule optical switching by Beltram and colleagues (*7*, *8*). More recently Blum et al. (*40*) have shown further heterogeneity in YFP fluorescence and have detected species that exhibit blue- and red-shifted emission compared with the dominant 527 nm emission.

Relating these kinetically defined states with structure remains elusive. The chromophore in the YFP−H148G has an exposed phenolic oxygen (*22*) and would seem available for rapid protonation. The overall p*K* of YFP-H148G differs only by 1 compared with the 10C variant studied here, where H148 is hydrogen-bonded to the phenolate ion. It seems likely that protonation of the phenolate group in YFP 10C is rapid (step 1a in Scheme 2) but there is a slow rearrangement of protons within the chromophore hydrogen bond network, and/or the p-hydroxybenzylideneimidazolidinone ring undergoes a cis−trans isomerization. The latter mechanism is an attractive possibility because it would be potentially very rapid in the excited state (*30*) and the protein structure may well undergo a rearrangement that traps the chromophore in trans isomer. This could be an explanation of the long-lived YFPHrb state (*8*).

The role of E222 is also intriguing. Previously, it was shown that photoconversion of wild-type GFP by 254 nm illumination was accompanied by decarboxylation of E222 (*27*). The photoconverted GFP had a high fluorescence, characteristic of the ionized state of the hydroxybenzylideneimidazolidinone ring. An E222Q GFP mutant also favored the strongly fluorescent ionized state (*41*). A related GFP from *Aequorea coerulescens* showed weak green fluorescence in its native form that was much enhanced in a E222G mutant (*42*). On the other hand, we found that on intense pulsed 532 nm irradiation, YFP lost 44 Da in mass, consistent with decarboxylation. This transformation was accompanied by photobleaching and conversion to the weakly fluorescent XFP state. Attempts to show that E222 was essential for YFP fluorescence emission were ambiguous because the E222A failed to undergo chromophore maturation.

In terms of applications of YFP as a probe in biological systems, our study highlights again the need to control pH and halide ion concentrations so as to maintain a dominant and constant proportion of the fluorescent YFP^- species in solution. Knowledge of the ground-state p*K* and protonation kinetics are helpful to interpret single molecule experiments, such as the determination landing rates and membrane protein dynamics, where blinking can give rise to false conclusions. Similarly in FRET experiments, blinking of a YFP acceptor needs to be distinguished from dynamics arising from distance and orientation changes relative to the donor. It is also important to control the illumination intensity because at high light levels, photons themselves act as catalysts of the protonation reaction. Under conditions where the net photobleaching rate exceeds 0.01 s^{-1} (i.e. around 1 min half time), the blinking rate will be significantly accelerated. Photobleaching can be used to advantage. The ability to bleach YFP reversibly opens up its use as a photoactivatable probe within living cells, to probe reactions on the seconds time scale (cf. *27*, *43*).

ACKNOWLEDGMENT

We thank Prof. W. E. Moerner and Dr. P. B. Conibear for discussions and Dr. J. Basra for assistance with diode array measurements. We thank the University of Leicester Biomedical Joint Workshop for help in construction of the TIRF microscope.

SUPPORTING INFORMATION AVAILABLE

Figure to show stopped-flow pH jump in the absence of Cl^- ions; derivation of eq 1; comparison of interpretation of states with previous literature. This material is available free of charge via the Internet at http://pubs.acs.org.

REFERENCES

1. Tsien, R. Y. (1998) The green fluorescent protein, *Annu. Rev. Biochem. 67*, 509−544.

2. Chattoraj, M., King, B. A., Bublitz, G. U., and Boxer, S. G. (1996) Ultrafast excited-state dynamics in green fluorescent protein: multiple states and proton transfer, *Proc. Natl. Acad. Sci. U.S.A. 93*, 8362−8367.
3. Creemers, T. M. H., Lock, A. J., Subramaniam, V., Jovin, T. M., and Volker, S. (2002) Red-shifted mutants of green fluorescent protein: reversible photoconversions studied by hole-burning and high-resolution spectroscopy, *Chem. Phys. 275*, 109−121.
4. Schwille, P., Kummer, S., Heikal, A. A., Moerner, W. E., and Webb, W. W. (2000) Fluorescence correlation spectroscopy reveals fast optical excitation- driven intramolecular dynamics of yellow fluorescent proteins, *Proc. Natl. Acad. Sci. U.S.A. 97*, 151−156.
5. Zumbusch, A., and Jung, G. (2000) Single molecule spectroscopy of the green fluorescent protein: a critical assessment, *Single Molecules 1*, 261−270.
6. Dickson, R. M., Cubitt, A. B., Tsien, R. Y., and Moerner, W. E. (1997) On/off blinking and switching behaviour of single molecules of green fluorescent protein, *Nature 388*, 355−358.
7. Cinelli, R. A. G., Pellegrini, V., Ferrari, A., Faraci, P., Nifosi, R., Tyagi, M., Giacca, M., and Beltram, F. (2001) Green fluorescent proteins as optically controllable elements in bioelectronics, *Appl. Phys. Lett. 79*, 3353−3355.
8. Nifosi, R., Ferrari, A., Arcangeli, C., Tozzini, V., Pellegrini, V., and Beltram, F. (2003) Photoreversible dark state in a tristable green fluorescent protein variant, *J. Phys. Chem. B 107*, 1679−1684.
9. Peterman, E. J. G., Brasselet, S., and Moerner, W. E. (1999) The fluorescence dynamics of single molecules of green fluorescent protein, *J. Phys. Chem. A 103*, 10553−10560.
10. Miyawaki, A., and Tsien, R. Y. (2000) Monitoring protein conformations and interactions by fluorescence resonance energy transfer between mutants of green fluorescent protein, *Methods Enzymol. 327*, 472−500.
11. Wakelin, S., Conibear, P. B., Woolley, R. J., Floyd, D. N., Bagshaw, C. R., M., K., and Malnasi-Csizmadia, A. (2002) Engineering Dictyostelium discoideum myosin II for the introduction of site-specific probes, *J. Muscle Res. Cell Motil. 24*, 673−683.
12. Malnasi-Csizmadia, A., Woolley, R. J., and Bagshaw, C. R. (2000) Resolution of conformational states of Dictyostelium myosin II motor domain using tryptophan (W501) mutants: Implications for the open-closed transition identified by crystallography, *Biochemistry 39*, 16135−16146.
13. Glasoe, P. K., and Long, F. A. (1960) Use of glass electrodes to measure acidities in deuterium oxide, *J. Phys. Chem. 64*, 188−190.
14. Pearson, D. S., Holtermann, G., Ellison, P., Cremo, C., and Geeves, M. A. (2002) A novel pressure jump apparatus for the microvolume analysis of protein- ligand and protein−protein interactions: Application to nucleotide binding to skeletal and smooth muscle myosin subfragment 1, *Biochem. J. 15*, 643−651.
15. Stanley, R. J., and Boxer, S. G. (1995) Oscillations in the Spontaneous Fluorescence From Photosynthetic Reaction Centers, *J. Phys. Chem. 99*, 859−863.
16. Gustavsson, T., Cassara, L., Gulbinas, V., Gurzadyan, G., Mialocq, J. C., Pommeret, S., Sorgius, M., and van der Meulen, P. (1998) Femtosecond spectroscopic study of relaxation processes of three amino-substituted coumarin dyes in methanol and dimethyl sulfoxide, *J. Phys. Chem. A 102*, 4229−4245.
17. Conibear, P. B., Kuhlman, P. A., and Bagshaw, C. R. (1998) Measurement of ATPase activities of myosin at the level of tracks and single molecules, *Adv. Exp. Med. Biol. 453*, 15−26.
18. Conibear, P. B., and Bagshaw, C. R. (2000) A comparison of optical geometries for combined flash photolysis and total internal reflection fluorescence microscopy, *J. Microsc. 200*, 218−229.
19. Axelrod, D., Burghardt, T. P., and Thompson, N. L. (1984) Total internal reflection fluorescence, *Annu. Rev. Biophys. Bioeng. 13*, 247−268.
20. Wakelin, S., and Bagshaw, C. R. (2003) A prism combination for near isotropic fluorescence excitation by total internal reflection, *J. Microsc. 209*, 143−148.
21. Press, W. H., Flannery, B. P., Teukolsky, S. A., and Vetterling, W. T. (1986) *Numerical Recipes: the art of scientific computing*, Cambridge University Press, Cambridge, U.K.
22. Wachter, R. M., Elsliger, M. A., Kallio, K., Hanson, G. T., and Remington, S. J. (1998) Structural basis of spectral shifts in the yellow-emission variants of green fluorescent protein, *Structure 6*, 1267−1277.
23. Wachter, R. M., and Remington, S. J. (1999) Sensitivity of the yellow variant of green fluorescent protein to halides and nitrate, *Curr. Biol. 9*, R628−R629.
24. Kovacs, M., Malnasi-Csizmadia, A., Woolley, R. J., and Bagshaw, C. R. (2002) Analysis of Nucleotide Binding to Dictyostelium Myosin II Motor Domains Containing a Single Tryptophan Near the Active Site, *J. Biol. Chem. 277*, 28459−28467.
25. Disteche, A. (1972) Effects of pressure on the dissociation of weak acids, *Symp. Soc. Exp. Biol. 26*, 27−60.
26. Volkmer, A., Subramaniam, V., Birch, D. J. S., and Jovin, T. M. (2000) One- and two-photon excited fluorescence lifetimes and anisotropy decays of Green Fluorescent Proteins, *Biophys. J. 78*, 1589−1598.
27. van Thor, J. J., Gensch, T., Hellingwerf, K. J., and Johnson, L. N. (2002) Phototransformation of green fluorescent protein with UV and visible light leads to decarboxylation of glutamate 222, *Nat. Struct. Biol. 9*, 37−41.
28. Visser, N. V., Hink, M. A., Borst, J. W., van der Krogt, G. N., and Visser, A. J. (2002) Circular dichroism spectroscopy of fluorescent proteins, *FEBS Lett. 521*, 31−35.
29. Scully, A. D., Matsumoto, A., and Hirayama, S. (1991) A Time-Resolved Fluorescence Study of Electronic Excitation- Energy Transport in Concentrated Dye Solutions, *Chem. Phys. 157*, 253−269.
30. Weber, W., Helms, V., McCammon, J. A., and Langhoff, P. W. (1999) Shedding light on the dark and weakly fluorescent states of green fluorescent proteins, *Proc. Natl. Acad. Sci. U.S.A. 96*, 6177−6182.
31. Jayaraman, S., Haggie, P., Wachter, R. M., Remington, S. J., and Verkman, A. S. (2000) Mechanism and cellular applications of a green fluorescent protein-based halide sensor, *J. Biol. Chem. 275*, 6047−6050.
32. Kneen, M., Farinas, J., Li, Y., and Verkman, A. S. (1998) Green fluorescent protein as a noninvasive intracellular pH indicator, *Biophys. J. 74*, 1591−1599.
33. Mallik, R., Udgaonkar, J. B., and Krishnamoorthy, G. (2003) Kinetics of proton transfer in a green fluorescent protein: a laser-induced pH jump study, *Proc. Indian Acad. Sci. 115*, 307−317.
34. Pierce, D. W., and Vale, R. D. (1999) Single-molecule fluorescence detection of green fluorescence protein and application to single-protein dynamics, *Methods Cell Biol. 58*, 49−73.
35. Pierce, D. W., Hom-Booher, N., and Vale, R. D. (1997) Imaging individual green fluorescent proteins, *Nature 388*, 338.
36. Cleland, W. W. (1975) Partition analysis and the concept of net rate constants as tools in enzyme kinetics, *Biochemistry 14*, 3220−3224.
37. Taylor, K. B. (2002) *Enzyme kinetics and mechanisms*, Kluwer Academic Publishers, Dordrecht, The Netherlands.
38. Shimomura, O. (1979) Structure of the Chromophore of *Aequorea* Green Fluorescent Protein, *FEBS Lett. 104*, 220−222.
39. Niwa, H., Inouye, S., Hirano, T., Matsuno, T., Kojima, S., Kubota, M., Ohashi, M., and Tsuji, F. I. (1996) Chemical nature of the light emitter of the *Aequorea* green fluorescent protein, *Proc. Natl. Acad. Sci. U.S.A. 93*, 13617−13622.
40. Blum, C., Meixner, A. J., and Subramaniam, V. (2004) Room temperature spectrally resolved single-molecule spectroscopy reveals new spectral forms and photophysical versatility of aequorea green fluorescent protein variants, *Biophys. J. 87*, 4172−4179.
41. Jung, G., Wiehler, J., Gohde, W., Tittel, J., Basche, T., Steipe, B., and Brauchle, C. (1998) Confocal microscopy of single molecules of the green fluorescent protein, *Bioimaging 6*, 54−61.
42. Gurskaya, N. G., Fradkov, A. F., Pounkova, N. I., Staroverov, D. B., Bulina, M. E., Yanushevich, Y. G., Labas, Y. A., Lukyanov, S., and Lukyanov, K. A. (2003) Colourless green fluorescent protein homologue from the non- fluorescent hydromedusa Aequorea coerulescens and its fluorescent mutants, *Biochem. J. 373*, 403−408.
43. Patterson, G. H., and Lippincott-Schwartz, J. (2002) A photoactivatable GFP for selective photolabeling of proteins and cells, *Science 297*, 1873−1877.

BI047581F